C. R. Physique 17 (2016) 861–873

Contents lists available at ScienceDirect

Comptes Rendus Physique

www.sciencedirect.com

Polariton physics / Physique des polaritons

Ultra-strong light–matter coupling and superradiance using dense electron gases

Couplage ultra-fort lumière–matière et superradiance avec un gaz dense d'électrons

Angela Vasanelli *, Yanko Todorov, Carlo Sirtori

Université Paris-Diderot, Sorbonne Paris Cité, Laboratoire "Matériaux et phénomènes quantiques", UMR 7162, 75013 Paris, France

ARTICLE INFO

Article history:
Available online 31 May 2016

Keywords:
Polariton
Plasmon
Semiconductor quantum well
Light–matter interaction
Superradiance
Patch microcavities

Mots-clés :
Polariton
Plasmon
Puits quantiques de semiconducteur
Interaction lumière–matière
Superradiance
Microcavités patch

ABSTRACT

The physics of the interaction between a dense two-dimensional electron gas and a microcavity photonic mode is reviewed. For high electronic densities, this system enters the ultra-strong coupling regime in which the Rabi energy, which measures the strength of the light–matter coupling, is of the same order of magnitude as the matter excitation. The ultra-strong coupling has been experimentally demonstrated by inserting a highly doped semiconductor layer between two metal plates that produce a microcavity, with extreme sub-wavelength confinement of the electromagnetic field. A record value at room temperature (73%) of the ratio between the Rabi and the matter excitation energies (the relative Rabi energy) has been measured together with a very large photonic gap induced by the polariton splitting. The ultra-strong coupling is a manifestation of a huge cooperative dipole, which is proportional to the number of electrons participating in the interaction. Such a phenomenal interaction with light appears also in the absence of a microcavity and, for a dipole coupled with free space, it gives rise to superradiance.

RÉSUMÉ

Nous passons en revue la physique de l'interaction entre un gaz bidimensionnel d'électrons et un mode photonique de microcavité. Pour des densités électroniques suffisamment grandes, le système rentre dans le régime de couplage ultra-fort, dans lequel l'énergie de Rabi, qui mesure l'intensité du couplage lumière–matière, est du même ordre de grandeur que l'excitation dans la matière. Le couplage ultra-fort a été démontré expérimentalement en insérant un semiconducteur fortement dopé entre deux couches métalliques, qui forment une cavité avec un confinement très sub-longueur d'onde du champ électromagnétique. À température ambiante, une valeur record (73 %) du rapport entre l'énergie de Rabi et celle de l'éxcitation électronique (l'énergie de Rabi relative) a été mesurée, ainsi qu'une large bande interdite photonique induite par l'anticroisement entre les branches polaritoniques. Le couplage ultra-fort est une manifestation de l'existence d'un dipôle coopératif, proportionnel au nombre d'électrons qui participent à l'interaction avec la

* Corresponding author.
E-mail address: angela.vasanelli@univ-paris-diderot.fr (A. Vasanelli).

http://dx.doi.org/10.1016/j.crhy.2016.05.001

lumière. Ce très fort couplage apparaît aussi en l'absence d'une microcavité et, dans le cas d'un dipôle couplé à l'espace libre, donne lieu au phénomène de superradiance.

1. Introduction

Ultra-strong light–matter coupling is a regime of cavity quantum electrodynamics, reached when the light–matter coupling energy, the Rabi energy E_R, is of the same order of magnitude as that of the matter excitation, E_{matter}, or of the cavity photon, E_c [1]. In this case, the routinely invoked rotating wave approximation is no longer applicable and the light–matter interaction Hamiltonian has to include anti-resonant and quadratic terms. As a consequence, new quantum phenomena and fascinating effects appear, ranging from dynamical Casimir effect [2,3] to superradiant phase transitions [4,5], efficient light emission [6–8], modified photon blockade [9], extraordinary conductance [10–12], cavity-assisted chemical and thermodynamic effects [13].

The first experimental observation of the ultra-strong coupling regime has been obtained by coupling an electronic excitation between confined levels in a quantum well (intersubband excitation) and a microcavity mode [14,15]. The quasiparticles issued from this coupling are called intersubband polaritons [16,17]. Thanks to the versatile engineering of the doping and of the electronic confinement, intersubband polaritons can display high values of the relative Rabi energy, i.e. the ratio between the Rabi and the matter excitation energies, E_R/E_{matter}. As a matter of fact, ultra-strong coupling regime has been demonstrated with intersubband polaritons in both the mid-infrared [14,18–22] and the THz range [15,23,24], by using different cavity geometries, from planar microcavities based on a dielectric confinement, to plasmonic microcavities displaying a highly subwavelength photon confinement.

Today, the ultra-strong coupling regime with a microcavity mode has been observed in several other material systems: superconducting circuits [25,26], cyclotron transitions [27], and cyclotron plasma [28], Frenkel molecular excitons [29,30], dye molecules [31,32].

In this review article, we will focus on intersubband polaritons, which are a system of choice for studying the fundamental properties of the ultra-strong coupling regime and its applications in photonics. That can be found in devices operating in the strong and ultra-strong coupling regime, where intersubband quantum engineering merges with photonic confinement to realize, for instance, quantum-well infrared photodetectors [33,34] and electrically pumped emitters [35–39]. Moreover, in this class of devices, there is a still underexplored link between electronic transport and quantum optics, which is now the object of investigation for organic systems coupled in plasmonic structures [10].

Another property of our system that has attracted much attention in the past few years is the bosonic character of intersubband polaritons [40]. Indeed, their interaction with optical phonons [38] may be exploited to realize devices based on stimulated emission of polaritons [40,41], following the same operation principle as exciton polariton lasers [42,43].

Finally, it must be pointed out that intersubband transitions in quantum wells are also suitable to be strongly coupled with the modes of plasmonic metasurfaces [44–46], giving rise to giant non-linear susceptibilities [47,48]. Coherent perfect absorption has been also observed in a photonic crystal resonator in the presence of a coupling with intersubband excitations [49].

Here we will review the basic concepts and some of the experimental results on the ultra-strong coupling between intersubband excitations in highly doped quantum wells and cavity modes. In sections 2 and 3, we will discuss the main properties of intersubband transitions and their coupling with cavity modes. Then, in section 4 we will present the properties of photon confinement in metal–dielectric–metal microcavities and we will justify why these cavities are particularly suitable for the observation of the ultra-strong coupling regime with intersubband excitations. The observation of the ultra-strong coupling regime with record values of the relative Rabi energy (73%) at room temperature will also be reviewed. The origin of such a high value of the relative Rabi energy can be ascribed to the fact that intersubband excitations in highly doped quantum wells display an extremely large collective dipole that almost perfectly overlaps with the photonic mode. We will show in section 5 that another way to probe the large dipole of collective intersubband excitations is the study of their decay into free-space radiation: a phenomenon called superradiance, recently observed in highly doped quantum wells [50]. Finally, we will discuss some perspectives in the field of intersubband polaritonics in the ultra-strong coupling regime.

2. Collective electronic excitations in quantum wells

Our system, conversely to those discussed in most of the articles of this issue, is based on n-doped semiconductor quantum wells, in which doping produces excess electrons. The left-hand part of Fig. 1 presents a sketch of the conduction band profile of a quantum well, confining electrons in the growth direction. As electrons are free in the layer plane, they display an approximately parabolic dispersion as a function of the in-plane momentum, as shown in the right-hand part of

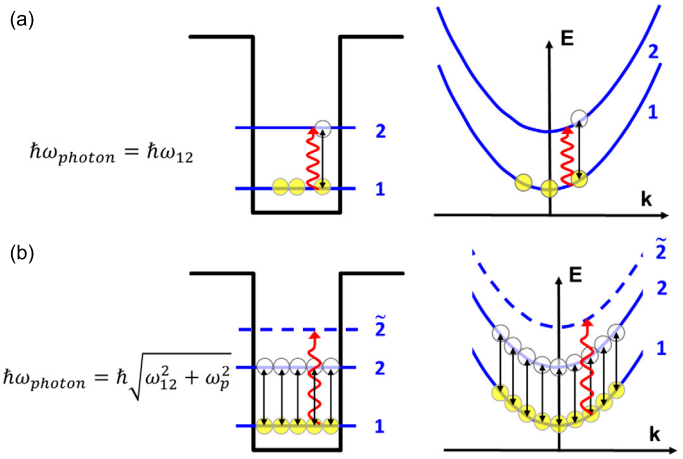

Fig. 1. Single particle (a) and many-body (b) intersubband transitions in the real (left side) and in the reciprocal (right side) space. (a) In a slightly doped quantum well, an intersubband absorption is a single particle transition that takes place between the ground and first excited state. (b) In a highly doped quantum well, there is a mutual interaction of all the dipolar oscillators at energy E_{12}. This interaction results in a blue shift of the intersubband absorption, which is centered at energy $\hbar\tilde{\omega}_{12} = \hbar\sqrt{\omega_{12}^2 + \omega_{P_{12}}^2}$.

the figure. The confined energy levels are called subbands. In the following, we will only consider intersubband transitions within the conduction band of a doped quantum well.

Transitions between the ground and first excited subband at energy $E_{12} = \hbar\omega_{12} = E_2 - E_1$ can take place in the presence of an electromagnetic field along the growth direction [51]. Such an intersubband transition corresponds to a polarization of the medium, hence to a collection of optical dipoles, along the growth direction z. We can associate with this dipole an oscillator strength $f_{12} = \frac{2m^*\omega_{12}}{\hbar}|z_{12}|^2$ with $|z_{12}|^2$ the square modulus of the dipole matrix element. Assuming a constant effective mass for all energies, the parabolic approximation (see ref. [52] for the non-parabolic case), the oscillator strength verifies the sum rule $\sum_j f_{ij} = 1$ valid for any initial state i, with the sum extending over all possible final states j. In the limit case of an infinite quantum well, only parity-changing transitions are allowed due to the symmetry of the potential. For the transition from the ground to the first excited state, one has $f_{12} = 0.96$, which almost saturates the sum rule. More generally, in a square quantum well, transitions between consecutive states (i.e. $j = i + 1$) are the most relevant ones [51].

In lightly doped quantum wells, light–matter interaction can be described by a single particle picture, where transitions between subbands are dictated by the dipole matrix elements between electronic states. In the parabolic approximation, the transition energy is the same for all the in-plane electron momenta **k**, as sketched on the right side of Fig. 1a, such that the typical intersubband absorption spectrum is a Lorentzian function centered at energy E_{12}. The absorption amplitude is proportional to $f_{12}(N_1 - N_2)$, where N_1 (respectively N_2) is the electronic density per unit surface in the ground subband (resp. first excited).

Nevertheless, intersubband absorption typically involves a huge number of electrons, with densities that can reach up to 10^{13} cm^{-2}. It is thus an intrinsically collective phenomenon, and its many-body nature has been the object of a vast literature [53]. The most important manifestation of this collective character is the fact that, in the presence of electromagnetic radiation, each electron feels an effective field induced by the excitation of the other electrons, called depolarization field [51,53]. The effect of the depolarization field is sketched in Fig. 1b: the coupling between the different intersubband dipoles results in a blue-shift of the intersubband resonance with respect to the transition energy E_{12}, corresponding to the excitation of a collective mode of the system, the intersubband plasmon [54]. The absorption spectrum is thus centered in this case at energy: $\tilde{E}_{12} = \sqrt{E_{12}^2 + E_{P_{12}}^2}$, where $E_{P_{12}}$ is the plasma energy of the $1 \to 2$ transition, defined as:

$$E_{P_{12}} = \hbar\omega_{P_{12}} = \hbar\sqrt{\frac{e^2(N_1 - N_2)f_{12}}{\varepsilon_0\varepsilon_s m^* L_{\text{eff}}}} \tag{1}$$

where L_{eff} is the effective length of interaction between the intersubband dipoles and the electromagnetic field [53]. The effect of the depolarization field is also shown in Fig. 2a, where the calculated absorption spectrum (blue line) of a GaAs/$Al_{0.45}Ga_{0.55}$As quantum well with an electronic density $N_s = 1.4 \times 10^{12}$ cm^{-2} in the ground subband, is compared with the corresponding spectrum expected in the single-particle approximation (red line).

The effect of the depolarization field is even more spectacular in a highly doped quantum well with several occupied subbands. In this case, depicted in Fig. 2b, the absorption spectrum consists of a single resonance (blue line), whose energy is completely different from those of the bare intersubband transitions (visible in the single-particle spectrum, red line) [21, 55]. The absorption resonance corresponds to the excitation of a collective mode of the system, the multisubband plasmon, resulting from the phase locking of all the different intersubband dipoles and concentrating almost the entire oscillator

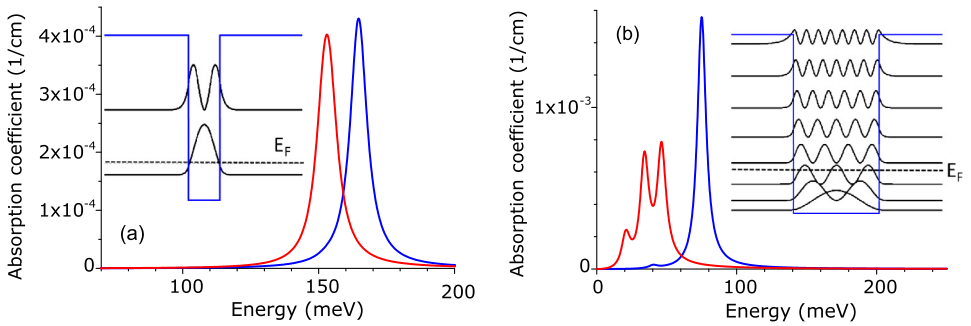

Fig. 2. Calculated absorption spectra in single-particle approximation (red line) and including the depolarization field (blue line), together with the conduction band profile and the square moduli of the electronic wavefunctions (inset) for two $GaAs/Al_{0.45}Ga_{0.55}As$ quantum wells of different thicknesses and same electronic density per unit volume $N_v = 2 \times 10^{18}$ cm^{-3}. The Fermi energy is indicated by a dashed line. Panel (a) presents the calculated spectra for a 7-nm quantum well: in the single particle approximation, the spectrum is centered at energy E_{12}, and undergoes a depolarization shift to energy $\tilde{E}_{12}$. The spectra in panel (b) have been obtained for a larger quantum well, 25 nm in thickness. In this case, the single-particle spectrum presents three resonances, corresponding to transitions $1 \to 2$, $2 \to 3$ and $3 \to 4$. The many-body spectrum shows the emergence of a unique bright resonance, corresponding to the excitation of a bright multisubband plasmon.

strength of the system. We have shown [22] that the energy of the multisubband plasmon E_{MSP} in a square quantum well can be written in analogy with the case, discussed above, of a single occupied subband:

$$E_{MSP} = \sqrt{E_{ISB}^2 + (\hbar\Omega_P)^2} \tag{2}$$

The intersubband contribution, E_{ISB}, is the harmonic mean of the squared intersubband transition energies weighted by their plasma energy:

$$E_{ISB}^2 = \frac{\hbar^2 \sum_\alpha \omega_{P_\alpha}^2}{\sum_\alpha \frac{\omega_{P_\alpha}^2}{\omega_\alpha^2}} \tag{3}$$

where the sum runs over all possible intersubband transitions $\alpha = j \to j+1$ between consecutive subbands. Ω_P is the effective plasma frequency [21], associated with the bright multisubband mode, obtained by adding all the contributions from the intersubband transitions involved in the interaction with light:

$$(\Omega_P)^2 = \sum_\alpha \omega_{P_\alpha}^2 \tag{4}$$

The last equation expresses the redistribution of the oscillator strength of each single electronic transition ($\propto \omega_{P_\alpha}^2$) into the sole bright multisubband plasmon mode [55].

Fig. 3 presents the evolution of the multisubband plasmon energy and of the intersubband contribution in a $GaAs/Al_{0.45}Ga_{0.55}As$ quantum well of increasing thickness for a fixed electronic density per unit volume $N_v = 2 \times 10^{18}$ cm^{-3}. As N_v is fixed, the plasma contribution to the multisubband plasmon energy is approximately constant (it varies between 61 and 66 meV). On the contrary, the intersubband contribution goes to zero for increasingly wide quantum wells, as the intersubband transition energies are vanishingly small. In this case, Ω_P tends towards the plasma frequency of a three-dimensional electron gas of density N_v. If the thickness of the doped semiconductor layer along the growth direction L is smaller than the wavelength in the semiconductor, the response of the three-dimensional electron gas to a radiation polarized along the growth direction consists of a well defined resonance at the plasma frequency, known as Berreman mode [56,57]. Fig. 3 thus schematizes the crossover from an intersubband (Fig. 2a) to a multisubband (Fig. 2b) plasmon, up to a Berreman mode, when varying the thickness of the quantum well while keeping constant the electronic density per unit volume. This crossover has also been investigated from an experimental point of view in reference [22].

3. Strong and ultra-strong coupling between a collective electronic excitation and a cavity mode

In order to describe from a theoretical point of view the coupling between intersubband transitions and a cavity mode, it is important to treat on the same footing the effect of the depolarization and of the electromagnetic field. This can be done by writing the light–matter interaction Hamiltonian in the dipole representation of the Coulomb gauge [58]. In this representation, the interaction Hamiltonian H_{int} is written in terms of the intersubband polarization density operator $\mathbf{P}$ as:

$$H_{int} = \int \frac{1}{\varepsilon_0 \varepsilon_s} \left(-\mathbf{D} \cdot \mathbf{P} + \frac{1}{2}\mathbf{P}^2 \right) d^3\mathbf{r} = H_{l-p} + H_p \tag{5}$$

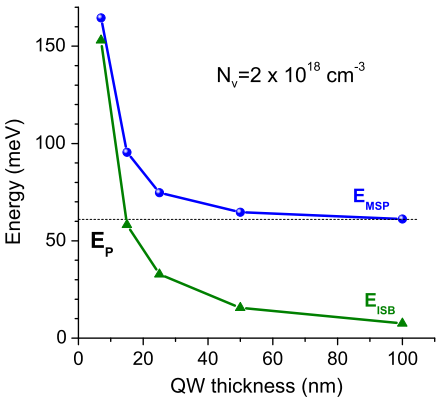

Fig. 3. Crossover from an intersubband to a multisubband plasmon, up to a Berreman mode, when varying the thickness of the quantum well while keeping constant the electronic density per unit volume. The blue line presents the energy of the absorption resonance E_{MSP} (see Eq. (2)), the green line the intersubband contribution (defined by Eq. (3)). Both are calculated for a fixed plasma contribution (horizontal dashed line) as a function of the quantum well thickness. The calculation has been performed for a GaAs/$Al_{0.45}Ga_{0.55}$As quantum well with fixed electronic density per unit volume $N_{\mathrm{v}} = 2 \times 10^{18}$ cm^{-3}.

where ε_{s} is the background dielectric constant and **D** is the displacement field operator. The Hamiltonian (5) is composed of two terms: H_{p} describes the polarization self-interaction, i.e. the dipole–dipole interaction between intersubband oscillators, $H_{\mathrm{l-p}}$ is responsible for the coupling between the multisubband plasmon and its electromagnetic environment.

The complete Hamiltonian of the system, composed by an ensemble of intersubband excitations interacting with a cavity mode at energy E_{c}, is:

$$H = \sum_{\alpha} \hbar\omega_{\alpha} B_{\alpha}^{\dagger} B_{\alpha} + E_{\mathrm{c}} \left(a^{\dagger} a + 1/2 \right) + H_{\mathrm{int}} \tag{6}$$

where the operators $B_{\alpha}^{\dagger}$, B_{α} are bosonic creation and annihilation operators of the intersubband transitions at frequency ω_{α}, while $a^{\dagger}$ (a) is the creation (annihilation) operator of the photon mode.

The diagonalization of this Hamiltonian is performed in two steps. First we diagonalize the matter part of the Hamiltonian, describing the intersubband transitions and their mutual interaction through H_{p} [58]:

$$H_{\mathrm{pl}} = \sum_{\alpha} \hbar\omega_{\alpha} B_{\alpha}^{\dagger} B_{\alpha} + H_{\mathrm{p}} \tag{7}$$

As the dipole–dipole coupling induced by H_{p} is quadratic in the operators B_{α}, the Hamiltonian H_{pl} can be diagonalized through a Bogoliubov transformation to obtain its eigenmodes, the multisubband plasmons. In this work, we will only consider systems in which the entire interaction with light is concentrated into a unique "bright" MSP mode at energy E_{MSP}. Nevertheless, this formalism is suitable to describe all the plasmon modes in the system, including the dark plasmons, which can be excited by electron energy loss spectroscopy [59].

The second step of our calculation involves the coupling between the bright MSP and the cavity mode. By introducing the multisubband plasmon creation and annihilation operators $P_{\mathrm{MSP}}^{\dagger}$ and P_{MSP}, we can write the complete Hamiltonian of the system as [58]:

$$H = E_{\mathrm{c}} \left(a^{\dagger} a + 1/2 \right) + E_{\mathrm{MSP}} P_{\mathrm{MSP}}^{\dagger} P_{\mathrm{MSP}} + H_{\mathrm{l-p}} \tag{8}$$

Here the plasmon–cavity mode interaction is expressed as [58]:

$$H_{\mathrm{l-p}} = \mathrm{i} \frac{\hbar\Omega_{\mathrm{p}}}{2} \sqrt{f_{\mathrm{w}} \frac{E_{\mathrm{c}}}{E_{\mathrm{MSP}}}} \left(a - a^{\dagger} \right) \left(P_{\mathrm{MSP}} + P_{\mathrm{MSP}}^{\dagger} \right) \tag{9}$$

where $0 \leq f_{\mathrm{w}} \leq 1$ is the overlap between the photon mode and the matter polarization [15]. As the microscopic dipoles associated with the electronic excitations are oriented along the growth direction z, f_{w} can be calculated as the ratio between the electromagnetic energy contained in the z-component of the field in the quantum well region and the total electromagnetic energy:

$$f_{\mathrm{w}} = \frac{\int_{\mathrm{QW}} |D_z|^2 \, \mathrm{d}\mathbf{r}}{\int_{\mathrm{volume}} |\mathbf{D}|^2 \, \mathrm{d}\mathbf{r}} \tag{10}$$

where the integral at the numerator is intended on the quantum well volume, while that at the denominator is on the entire volume of the system.

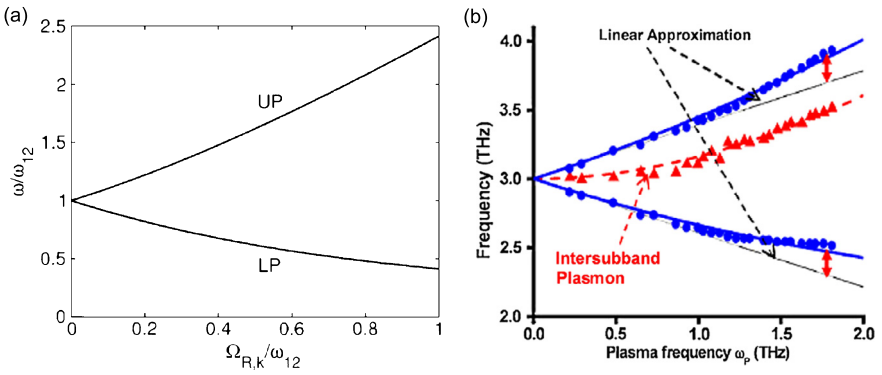

Fig. 4. (a) Extracted from ref. [1]. Frequency of the upper and lower polariton states calculated for $E_c = E_{12}$ in the ultra-strong coupling regime as a function of the Rabi frequency. All the frequencies are normalized to that of the intersubband transition ω_{12}. (b) Extracted from ref. [15]. Upper (UP) and lower (LP) polariton frequencies (in blue) as functions of the plasma frequency ω_P for $\omega_c = \omega_{12}$. The energy of the intersubband plasmon is also plotted (in red). In this plot, all symbols correspond to experimental data, while lines report the theoretical modeling of our results.

After diagonalization of the Hamiltonian (8), including the antiresonant terms, one gets the following secular equation, fulfilled by the polaritons, i.e. the new eigenmodes issued from the coupling [15,21,58]:

$$\left(E^2 - E_{MSP}^2\right)\left(E^2 - E_c^2\right) = E_R^2 E_c^2 \tag{11}$$

with E_R the Rabi energy. The last is proportional to the plasma energy through:

$$E_R = \hbar\,\Omega_P\sqrt{f_w} \tag{12}$$

Note that our formalism is suitable to describe intersubband and multisubband plasmons and, in the limit of large quantum wells, also Berreman modes. In the following we will generically indicate the energy of a collective electronic excitation as E_{matter}.

In the first theoretical article introducing the ultra-strong coupling regime [1], the resonance condition between an intersubband excitation (in the case of one occupied subband) and a cavity mode was defined as $E_{12} = E_c$, in analogy with the case of a two-level system coupled with a cavity mode. The ratio E_R/E_{12} was thus considered as a figure of merit of the ultra-strong coupling regime [1,18,14,15]. The crossover from the strong to the ultra-strong coupling regime was indeed studied by plotting the polariton energies at the "resonance" condition $E_c = E_{12}$ as a function of E_R/E_{12}, as shown in Fig. 4a. For $E_R/E_{12} \approx 0.3$, the upper and lower polariton energies deviate from the linear dependence typical of the strong coupling regime, due to the anti-resonant terms of the light–matter interaction. This non-linear behavior has also been demonstrated experimentally with THz intersubband polaritons [15,58], by changing the electronic density in the ground state of the quantum well (hence the plasma and the Rabi energy) through the temperature (see Fig. 4b).

However, the resonance condition needs to be redefined if the electronic density is so high that the plasma contribution is comparable to the intersubband one. Indeed, as discussed in the previous section, in this case the electronic excitation interacting with light is a collective mode, at a different energy E_{matter} with respect to the electronic transition energies. The resonance condition should thus be written as $E_c = E_{matter}$ and the figure of merit of the light–matter coupling is the ratio E_R/E_{matter}. The energies of the polariton states at the resonance condition $E_c = E_{matter}$, derived from Eq. (11), are thus given by:

$$\frac{E_{UP/LP}}{E_{matter}} = \sqrt{1 \pm \frac{E_R}{E_{matter}}} \tag{13}$$

This dependence is presented by the black line in Fig. 5a. In the limit $E_R/E_{matter} << 1$, Eq. (13) gives a linear dependence of the polariton states on the Rabi energy, which is typical of the strong coupling regime (red dashed line in Fig. 5a). As a consequence, also in the case of collective electronic excitations, the non-linear splitting, extracted from Eq. (13), is a signature of the ultra-strong coupling regime [1].

Fig. 5b presents the polariton energy, normalized to the matter excitation energy, E_{matter}, plotted for different values of E_R/E_{matter} as a function of the normalized cavity mode energy E_c/E_{matter}. From these curves, we can see that the polariton energies, and particularly those of the lower polariton branch, are significantly modified by the increase in the ratio E_R/E_{matter}. Indeed, while the horizontal asymptote of the upper polariton branch is E_{matter}, that of the lower polariton branch is $E_{min} = E_{matter}\sqrt{1 - (E_R/E_{matter})^2}$. Interestingly, the minimum energy splitting between the two branches occurs when $E_c = E_{min}$. This means that the lower branch can be pushed at arbitrarily low frequencies by increasing the ratio E_R/E_{matter} towards 1. This implies that a strong absorption resonance can be produced even in the far infrared. Furthermore, a photonic gap appears in the dispersion, whose width E_g is given by:

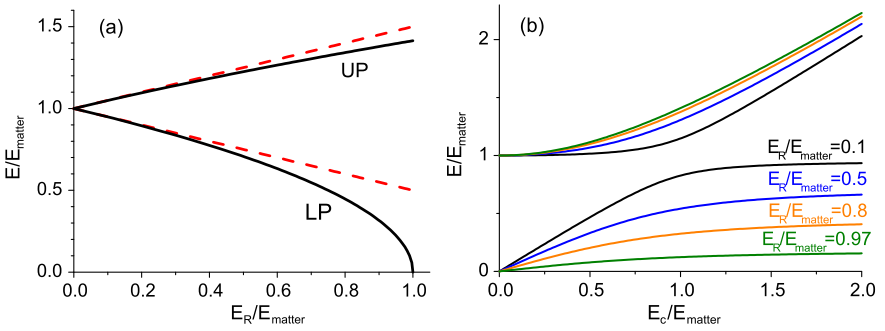

Fig. 5. (a) Energy of the upper and lower polariton states calculated at resonance ($E_c = E_{matter}$) in the ultra-strong (black line) and in the strong (red dashed line) coupling regime as a function of the Rabi energy. (b) Adapted from ref. [22]. Energy of the polariton branches as a function of the energy of the cavity mode. All the energies are normalized to that of the matter excitation. Four dispersion curves are shown, corresponding to different relative coupling strengths.

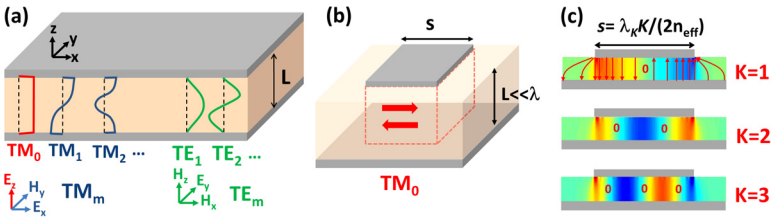

Fig. 6. (a) Metal–dielectric–metal waveguide of thickness L. The electric field distribution of the first transverse magnetic TM_m and transverse electric TE_m has been indicated. (b) Double-metal square patch microcavity. We have considered the regime of low frequencies where the thickness L is small compared to the photon wavelength, so that only the TM_0 mode is supported. In this regime, the apertures highlighted by dashed lines act as effective boundaries for the TM_0. (c) Vertical electric field distribution for the standing wave patterns along the x-direction. The integer K counts the nodes of the standing wave (indicated by a "0"). For $K = 1$, we have also sketched the electric field lines.

$$\frac{E_g}{E_{matter}} = 1 - \sqrt{1 - \left(\frac{E_R}{E_{matter}}\right)^2} \tag{14}$$

The width of the photonic gap can be adjusted by modifying E_R through the overlap with the cavity mode (f_w) and the density of the electron gas (which affects Ω_P and thus E_R). This property can be used to create materials with an artificial Reststrahlen band [22]. Indeed, the shape of the polaritonic dispersion is very similar to that observed when optical phonons are coupled with electromagnetic modes [60].

It is important to remark that as $f_w \leq 1$ and $E_P \leq E_{matter}$, there exists an upper limit for the coupling energy, $E_R/E_{matter} \leq 1$. This condition avoids unphysical values for the polariton energies in agreement with the no-go theorem for the electron gas coupled with a microcavity mode [4]. In other words, one could say that the ultimate limit of the ultra-strong coupling regime is achieved in metals, where the energy of the lower polariton branch vanishes, and the forbidden band spans from 0 to the plasma edge E_P.

4. Observation of the ultra-strong coupling regime: collective excitations in double metal patch microcavities

From Eq. (12), it clearly appears that two different quantities have to be controlled in order to achieve the ultra-strong coupling regime: the ratio $\hbar\Omega_P/E_{matter}$ and the factor f_w. The first quantity depends on the confinement potential and on the density of the electron gas, as discussed in relation to Fig. 3. Berreman modes are particularly interesting for achieving the ultra-strong coupling regime, as they are characterized by a negligible intersubband contribution, such that $\hbar\Omega_P \approx E_{matter}$.

The factor f_w only depends on the geometry of the cavity, as it describes the overlap between the cavity mode and the electron gas. All – dielectric [17] and hybrid metal – dielectric [61,18,35] cavities were first employed to observe intersubband polaritons in the mid-infrared range, with a ratio E_R/E_{matter} up to 0.3. In order to increase this value, double-metal microcavities [62] have been proposed and realized both in the mid and in the far infrared.

These waveguides, reminiscent of the microstrip lines of microwave technology [63], were first employed for THz quantum cascade lasers [64]. In these structures, a dielectric layer of thickness L is sandwiched between two metals. Assuming an almost perfect metal, the eigenmodes of the structure appear as series of TM_m and of TE_m modes [65], with electric field distribution sketched in Fig. 6a. Of particular relevance is the lowest order TM_0 mode, which has an electric field D_z component that is almost homogeneous along the dielectric core, and thus perfectly fulfills the intersubband selection rule. Furthermore, the mode TM_0 has a linear dispersion that is independent of the thickness of the waveguide L. Following Eq. (10), the overlap factor between the TM_0 mode of a double-metal cavity of thickness L and an ensemble of N_{QW} doped

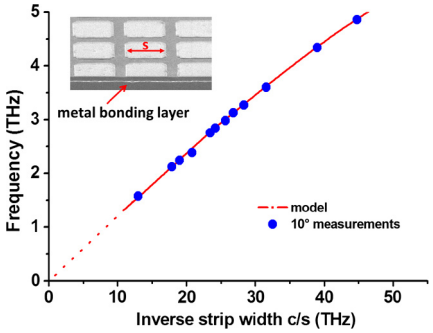

Fig. 7. Inset: Scanning electron microscope (SEM) picture of an array of patch micro-cavities, resonating in the THz range, with an indication of the Au–Au bonding layer that serves as a metal ground. Main panel: Frequency of the fundamental cavity mode as a function of the inverse patch dimension. The symbols present the reflectivity minima measured at 10°, while the continuous line shows the result of our model (Eq. (15)).

quantum wells is $f_w = N_{QW} \times L_{QW}/L$, where L_{QW} is the quantum well width. Very high values of f_w (≈ 0.6) can thus be reached by using thin barriers between the quantum wells [15].

Further lateral confinement of the photon field can be achieved by structuring the top metal of the waveguide. Fig. 6b presents the example of a square patch with side s. Such structures, reminiscent of RF patch antennas [63], operate in the regime where the thickness L is very small as compared to the wavelength. In that case, the only mode that propagates in the double-metal region is the TM_0 mode. Owing to their subwavelength dimensions, the apertures between the single-metal and double-metal regions (indicated with dashed line in Fig. 6b) act as effective boundaries for the TM_0 mode with very strong reflectivity [66]. The TM_0 wave that bounces back and forth between the boundaries then forms standing wave patterns as indicated in Fig. 6c. For instance, the standing waves along the x-direction have energies E_K provided by the equation:

$$E_K = \frac{\hbar c K}{2 n_{\text{eff}} s} \tag{15}$$

where c is the speed of light, K is an integer that counts the zeros of the electric field along the x-direction, and n_{eff} is an effective index, which is typically greater than the bulk refractive index of the dielectric layer [66].

In the inset of Fig. 7, we show a realization of arrays of such patch microcavities with GaAs layers. These structures are obtained by the Au–Au wafer bonding technique [67], where the lower bond layer serves as metallic ground. These arrays are probed through reflectivity measurements, such that the standing-wave modes appear as reflectivity dips. The main panel of Fig. 7 presents the frequency position of the reflectivity minima measured on a double metal patch microcavity as a function of the inverse microstrip width s, thus illustrating that the cavity mode energy can be tuned with $1/s$ following Eq. (15). The same cavity concept has been implemented in the mid-infrared frequency range, by downscaling the dimensions of the resonator [68], and even in the near infrared [69].

The highest value of the relative Rabi energy at room temperature in any quantum system has been obtained by coupling a Berreman mode with the fundamental TM_0 mode of a double-metal cavity, as reported in reference [22]. In this work, a 148-nm GaInAs layer, n-doped with an electronic density 7×10^{18} cm^{-3} and embedded between two AlInAs barriers, has been inserted into a double-metal cavity of total thickness 240 nm. The calculated overlap factor between the electron gas and the cavity mode is in this case $f_w = 0.53$. In order to vary the detuning between the cavity and the Berreman mode, square patches of different sizes have been realized, varying from $s = 0.65$ µm, confining the fundamental mode at $E_c = 250$ meV, to $s = 8$ µm, corresponding to $E_c = 20$ meV.

Fig. 8a presents reflectivity spectra measured at room temperature, at an incidence angle of 10° for different values of the patch dimensions. The energy of the reflectivity minima is plotted in Fig. 8b (bullets) as a function of the first-order cavity mode energies. The ultra-strong coupling with the Berreman mode results in the opening of a wide reflectivity band, delimited by the horizontal asymptotes of the upper and lower polariton branches, as predicted by our model presented in section 3. The Berreman mode energy, indicated by a star in Fig. 8b, fixes the upper bound of the polaritonic gap. From the data, we extract $E_{\text{min}} = 80$ meV and thus a vacuum Rabi energy $E_R = 86.7$ meV, corresponding to 73% of the matter excitation energy ($E_{MSP} = 118.2$ meV). Both this Rabi energy and the ratio E_R/E_{MSP} are the highest measured for intersubband polaritons.

When the lower polariton branch approaches the energies of GaInAs and AlInAs optical phonons, more anticrossing features are visible, demonstrating the existence of phonon–plasmon–polariton modes [70]. The solid blue lines in Fig. 8b present the simulated polaritonic dispersion, in excellent agreement with our data. As a comparison, the red dashed line presents the dispersion calculated without taking into account the coupling with the optical phonons. It has the same shape as the theoretical dispersion curves discussed in relation with Fig. 5, with a single anticrossing due to the interaction with the Berreman mode.

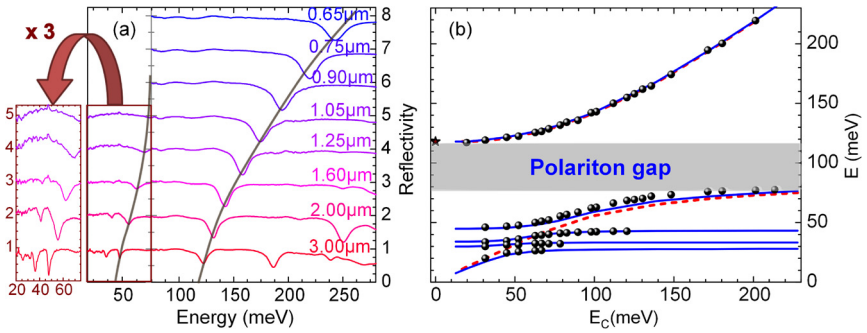

Fig. 8. Adapted from ref. [22]. (a) Set of chosen reflectivity spectra, offset for clarity, of the array of patches measured at room temperature. The brown rectangle indicates the part of the spectra that has been detected by a bolometer. In order to better evidence the reflectivity minima, the left-hand part of the figure shows a zoom where the signal has been multiplied by a factor of three. The magnified spectra have also been translated in order to keep the same baseline as in the right part of the figure. (b) Energy position of the reflectivity minima as a function of the fundamental cavity mode energy (bullets). The star indicates the energy of the Berreman mode as measured in transmission at Brewster angle. The blue lines present the simulated polaritonic dispersion by including the coupling with optical phonons. For comparison, the dashed red line presents the simulated dispersion by only including the coupling between the Berreman and the cavity modes.

An improved relative Rabi energy of 91% at room temperature has been recently measured in our group by thinning the AlInAs barriers and by etching the semiconductor layer between the metallic patches. This result will be reported in a forthcoming publication [71].

5. Observation of superradiance: collective excitations coupled with free-space radiation

The observation of the ultra-strong coupling regime in our system is intrinsically related to the possibility of locking together in phase through Coulomb interaction a huge number of electronic oscillators, giving rise to a collective dipole. The resulting electronic excitation, the multisubband plasmon, interacts with the electromagnetic field with a coupling energy proportional to the effective plasma energy (see Eq. (12)). The last is in turn proportional to the surface density of the electron gas, N_s. The cavity is a probe for this interaction, provided it entirely overlaps the spatial distribution of the collective mode.

In this section, we discuss a different way to probe the interaction of a collective electronic excitation with an electromagnetic field: its spontaneous decay into free space radiation. The spontaneous emission rate of a multisubband plasmon, evaluated using Fermi's golden rule, is expressed as [50,72]:

$$\Gamma(\theta) = \frac{e^2 N_s}{2 m^* c \epsilon_0 \sqrt{\epsilon_s}} \frac{\sin^2\theta}{\cos\theta} \tag{16}$$

where θ is the emission angle measured with respect to the normal to the quantum well plane. From this expression, we can see that the spontaneous emission rate depends on the density per unit surface of the electrons interacting with the electromagnetic field. This dependence is typical of the superradiance phenomenon. Superradiance, first introduced by Dicke in 1954 [73], is the coherent enhancement of the spontaneous emission rate of a quantum emitter owing to the presence in its vicinity of other identical emitters. It was observed in several systems, ranging from low-pressure optically pumped gases [74], to cold atomic gases [75], quantum dots [76], organic emitters [77], superconducting transmon qubits [78], and cyclotron resonances [79]. Superradiance occurs when a dense collection of emitters oscillates in phase: our system is thus ideal for the observation of this phenomenon, as it is based on a dense collection of dipolar oscillators, all oriented along the same direction (the confinement direction).

Fig. 9a, extracted from ref. [50], presents the calculated spontaneous emission time of a multisubband plasmon (red line) in a GaInAs quantum well, as a function of the electronic density per unit surface, at a fixed emission angle $\theta = 60°$. The blue line presents for comparison the radiative lifetime of a single emitter at the same energy as that of the multisubband plasmon. From this comparison, we can see that the superradiant character of the multisubband plasmon can give rise to a six orders of magnitude faster spontaneous emission in the mid infrared. Furthermore, uncommonly for an intersubband system, the spontaneous emission lifetime can be even shorter than the non-radiative lifetime (dashed horizontal line), such that radiative decay can be the dominant relaxation mechanism of the multisubband plasmon. As a consequence, the observation of a radiatively broadened and density dependent linewidth is a striking proof of the superradiant nature of the multisubband plasmon.

In reference [50], we presented a set of experimental data showing the radiative broadening of the multisubband plasmon and the consequent proof of its superradiant nature. We measured the emission of a multisubband plasmon, under the application of an in-plane current in a device based on the same geometry as a field effect transistor. We performed angle-resolved spectra of samples with different electronic densities. Some of these spectra are shown in Fig. 9b, measured at room temperature on three samples with different electronic densities for the same emission angle. From this graph, we

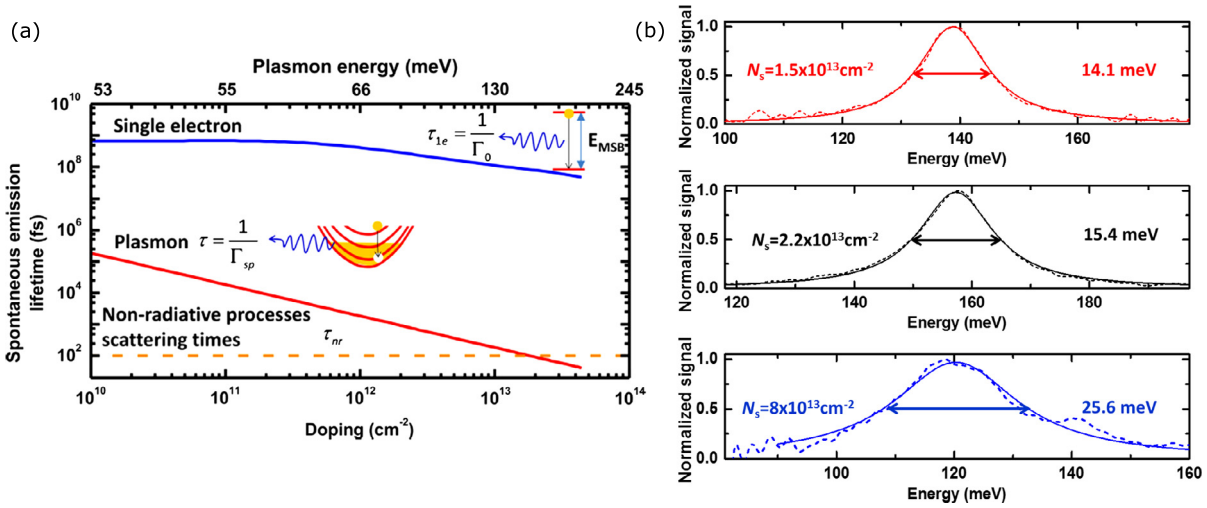

Fig. 9. (a) From reference [50]. Spontaneous emission time as a function of the electronic density for superradiant emission from the multisubband plasmon (red line, our case) at $\theta = 60°$ and a single two-level emitter (blue) with the same energy as the collective excitation. The dashed line indicates the typical nonradiative lifetime in intersubband systems. (b) Emission spectra measured on three quantum wells with different electronic densities at the same emission angle. The linewidth increases with the electronic density, demonstrating the superradiant character of the emission process.

can clearly see the radiative broadening associated with the increase in the electronic density, in agreement with Eq. (16). Our experimental observations are supported by a complete quantum model of the multisubband plasmon incandescent emission, based on the resolution of quantum Langevin equations in the input–output formalism [80].

6. Conclusions and perspectives

Electronic excitations in highly-doped semiconductors display a collective behavior when interacting with an electromagnetic field. This results in an enhanced light–matter interaction, with a coupling energy proportional to the density of the electrons involved. Two physical phenomena attest to this enhancement. The first one is the achievement of the ultra-strong coupling between the collective excitation and a microcavity mode displaying a good overlap with the electron gas (such as the fundamental mode of a double-metal microcavity). Record values of the relative Rabi energy have indeed been observed up to room temperature in this system [15,22]. The second phenomenon is the superradiant behavior of the collective electronic excitation, when decaying into the free-space radiation [50].

The demonstration of these two quantum effects with collective electronic excitations opens the way towards the realization of new optoelectronic devices combining many-body physics and quantum optics. To this aim, probably the most fascinating phenomenon to investigate, both from a theoretical and from an experimental point of view, is the interplay between electronic transport and ultra-strong coupling. Two different approaches can be followed: one can look for signatures of quantum optics on electronic transport, or, conversely, use an electrical current to resonantly excite a bosonic light–matter coupled state. Concerning the first approach, an important result has been recently achieved by the group of T.W. Ebbesen in organic semiconductors [10]. They measured the conductivity of organic semiconductors strongly coupled with the vacuum electromagnetic field on plasmonic structures. They demonstrated that the current can be increased by an order of magnitude at resonance, due to a delocalization of the wavefunctions of the hybridized light–matter states. The current enhancement due to a coupling with light has also been theoretically investigated by several groups [11,12,81]. The observed effect could be very important for applications, as it proposes a way to increase the mobility in disordered materials thanks to the coupling with light.

The interplay between electronic transport and quantum optics could also be studied in view of realizing devices based on the resonant electrical pumping of polaritons or superradiant states. These devices, taking advantage of the extremely short spontaneous emission time of collective electronic excitations, would be efficient cold mid-infrared emitters for several civil and military applications, such as environmental sensing, requiring broadband sources, and mid-infrared optical coherence tomography [82], requiring short coherence lengths.

Several efforts have already been done in this direction. The demonstration of an electroluminescent device based on intersubband polaritons [35] can be considered as a first step in the study of the effect of a current on the polaritonic emission. This kind of device stands on a quantum cascade structure inserted into a microcavity. The quantum cascade structure is designed so as to avoid population inversion: to this aim, thick extraction barriers are used to maintain an important electronic density in the ground state of a highly doped quantum well, even under the application of a bias voltage [83]. An electroluminescence signal from the lower polariton branch has been measured, whose energy position changes with the applied voltage, as a result of the coupling between the electronic component of the polariton state and the injector of the quantum cascade structure [36,37]. The coupling between the injector and the polariton states can be

designed through bandstructure engineering, which is a routinely used procedure to realize intersubband devices. As an example, reference [38] reports on an electrically pumped device, in which the upper polariton branch is populated by resonant tunneling, while the lower polariton branch is populated through upper polariton–LO-phonon scattering. The last observation also opens the way towards a new class of devices, based on stimulated emission of polaritons [40,41], following the same operation principle as exciton polariton lasers [42,43]. This could be particularly interesting for the THz domain, where the operation temperature of quantum cascade lasers [84] currently does not exceed 200 K [85].

It is important to underline that the typical densities necessary for the observation of superradiance and ultra-strong light–matter coupling with electronic excitations are typically employed in Si field effect transistors based on CMOS technology. The possibility of inserting quantum optics into CMOS electronics is an intriguing perspective, as it could enable novel functionalities, based on the use of mid- and far-infrared optical signals in existing electronic devices.

Acknowledgements

The contributions of Benjamin Askenazi, Aymeric Delteil, Pierre Jouy, Thibault Laurent, and Giulia Pegolotti have been extremely valuable for this review and they are greatly acknowledged by the authors. We also thank Isabelle Sagnes and Grégoire Beaudoin for growing the samples of our experiments. This work has been supported by the ERC grant "ADEQUATE".

References

[1] C. Ciuti, G. Bastard, I. Carusotto, Quantum vacuum properties of the intersubband cavity polariton field, Phys. Rev. B 72 (2005) 115303.
[2] S.D. Liberato, C. Ciuti, I. Carusotto, Quantum vacuum radiation spectra from a semiconductor microcavity with a time-modulated vacuum Rabi frequency, Phys. Rev. Lett. 98 (2007) 103602, http://dx.doi.org/10.1103/PhysRevLett.98.103602.
[3] A. Auer, G. Burkard, Entangled photons from the polariton vacuum in a switchable optical cavity, Phys. Rev. B 85 (2012) 235140, http://dx.doi.org/10.1103/PhysRevB.85.235140, http://link.aps.org/doi/10.1103/PhysRevB.85.235140.
[4] P. Nataf, C. Ciuti, No-go theorem for superradiant quantum phase transitions in cavity qed and counter-example in circuit qed, Nat. Commun. 1 (2010) 72, http://dx.doi.org/10.1038/ncomms1069.
[5] S. De Liberato, C. Ciuti, Quantum phases of a multimode bosonic field coupled to flat electronic bands, Phys. Rev. Lett. 110 (2013) 133603, http://dx.doi.org/10.1103/PhysRevLett.110.133603, http://link.aps.org/doi/10.1103/PhysRevLett.110.133603.
[6] C. Ciuti, I. Carusotto, Input–output theory of cavities in the ultrastrong coupling regime: the case of time-independent cavity parameters, Phys. Rev. A 74 (3) (2006) 033811.
[7] S.D. Liberato, C. Ciuti, Quantum model of microcavity intersubband electroluminescent devices, Phys. Rev. B 77 (2008) 155321, http://dx.doi.org/10.1103/PhysRevB.77.155321.
[8] S.D. Liberato, C. Ciuti, Quantum theory of electron tunneling into intersubband cavity polariton states, Phys. Rev. B 79 (2009) 075317.
[9] A. Ridolfo, M. Leib, S. Savasta, M.J. Hartmann, Photon blockade in the ultrastrong coupling regime, Phys. Rev. Lett. 109 (2012) 193602, http://dx.doi.org/10.1103/PhysRevLett.109.193602, http://link.aps.org/doi/10.1103/PhysRevLett.109.193602.
[10] E. Orgiu, J. George, J.A. Hutchison, E. Devaux, J.F. Dayen, B. Doudin, F. Stellacci, C. Genet, J. Schachenmayer, C. Genes, G. Pupillo, P. Samorì, T.W. Ebbesen, Conductivity in organic semiconductors hybridized with the vacuum field, Nat. Mater. 14 (2015) 1123.
[11] J. Feist, F.J. Garcia-Vidal, Extraordinary exciton conductance induced by strong coupling, Phys. Rev. Lett. 114 (2015) 196402.
[12] J. Schachenmayer, C. Genes, E. Tignone, G. Pupillo, Cavity-enhanced transport of excitons, Phys. Rev. Lett. 114 (2015) 196403, http://dx.doi.org/10.1103/PhysRevLett.114.196403, http://link.aps.org/doi/10.1103/PhysRevLett.114.196403.
[13] J.A. Hutchison, A. Liscio, T. Schwartz, A. Canaguier-Durand, C. Genet, V. Palermo, P. Samori, T.W. Ebbesen, Tuning the work-function via strong coupling, Adv. Mater. 25 (2013) 2481, http://dx.doi.org/10.1002/adma.201203682.
[14] G. Günter, A.A. Anappara, J. Hees, A. Sell, G. Biasiol, L. Sorba, S.D. Liberato, C. Ciuti, A. Tredicucci, A. Leitenstorfer, R. Huber, Sub-cycle switch-on of ultrastrong light–matter interaction, Nature 458 (2009) 178.
[15] Y. Todorov, A.M. Andrews, R. Colombelli, S.D. Liberato, C. Ciuti, P. Klang, G. Strasser, C. Sirtori, Ultrastrong light–matter coupling regime with polariton dots, Phys. Rev. Lett. 105 (2010) 196402.
[16] A. Liu, Rabi splitting of the optical intersubband absorption line of multiple quantum wells inside a Fabry–Pérot microcavity, Phys. Rev. B 55 (11) (1997) 7101.
[17] D. Dini, R. Köhler, A. Tredicucci, G. Biasiol, L. Sorba, Microcavity polariton splitting of intersubband transitions, Phys. Rev. Lett. 90 (12) (2003) 116401.
[18] A.A. Anappara, S.D. Liberato, A. Tredicucci, C. Ciuti, G. Biasiol, L. Sorba, F. Beltram, Signatures of the ultrastrong light–matter coupling regime, Phys. Rev. B 79 (2009) 201303(R).
[19] P. Jouy, A. Vasanelli, Y. Todorov, A. Delteil, G. Biasiol, L. Sorba, C. Sirtori, Transition from strong to ultra-strong coupling regime in mid-infrared metal–dielectric–metal cavities, Appl. Phys. Lett. 98 (23) (2011) 231114.
[20] M. Porer, J.-M. Ménard, A. Leitenstorfer, R. Huber, R. Degl'Innocenti, S. Zanotto, G. Biasiol, L. Sorba, A. Tredicucci, Nonadiabatic switching of a photonic band structure: ultrastrong light–matter coupling and slow-down of light, Phys. Rev. B 85 (2012) 081302, http://dx.doi.org/10.1103/PhysRevB.85.081302, http://link.aps.org/doi/10.1103/PhysRevB.85.081302.
[21] A. Delteil, A. Vasanelli, Y. Todorov, C.F. Palma, M.R. St-Jean, G. Beaudoin, I. Sagnes, C. Sirtori, Charge-induced coherence between intersubband plasmons in a quantum structure, Phys. Rev. Lett. 109 (2012) 246808.
[22] B. Askenazi, A. Vasanelli, A. Delteil, Y. Todorov, L.C. Andreani, G. Beaudoin, I. Sagnes, C. Sirtori, Ultra-strong light–matter coupling for designer Reststrahlen band, New J. Phys. 16 (2014) 043029.
[23] M. Geiser, F. Castellano, G. Scalari, M. Beck, L. Nevou, J. Faist, Ultrastrong coupling regime and plasmon polaritons in parabolic semiconductor quantum wells, Phys. Rev. Lett. 108 (2012) 106402, http://dx.doi.org/10.1103/PhysRevLett.108.106402, http://link.aps.org/doi/10.1103/PhysRevLett.108.106402.
[24] D. Dietze, K. Unterrainer, J. Darmo, Role of geometry for strong coupling in active terahertz metamaterials, Phys. Rev. B 87 (2013) 075324, http://dx.doi.org/10.1103/PhysRevB.87.075324, http://link.aps.org/doi/10.1103/PhysRevB.87.075324.
[25] T. Niemczyk, F. Deppe, H. Huebl, E.P. Menzel, F. Hocke, M.J. Schwarz, J.J. Garcia-Ripoll, D. Zueco, T. Hümmer, E. Solano, A. Marx, R. Gross, Circuit quantum electrodynamics in the ultrastrong-coupling regime, Nat. Phys. 6 (2010) 772, http://dx.doi.org/10.1038/nphys1730.
[26] D. Ballester, G. Romero, J.J. García-Ripoll, F. Deppe, E. Solano, Quantum simulation of the ultrastrong-coupling dynamics in circuit quantum electrodynamics, Phys. Rev. X 2 (2012) 021007, http://dx.doi.org/10.1103/PhysRevX.2.021007, http://link.aps.org/doi/10.1103/PhysRevX.2.021007.

[27] G. Scalari, C. Maissen, D. Turcinkova, D. Hagenmuller, S.D. Liberato, C. Ciuti, C. Reichl, D. Schuh, W. Wegscheider, M. Beck, J. Faist, Ultrastrong coupling of the cyclotron transition of a 2d electron gas to a THz metamaterial, Science 335 (2012) 1323, http://dx.doi.org/10.1126/science.1216022.
[28] V.M. Muravev, P.A. Gusikhin, I.V. Andreev, I.V. Kukushkin, Ultrastrong coupling of high-frequency two-dimensional cyclotron plasma mode with a cavity photon, Phys. Rev. B 87 (2013) 045307, http://dx.doi.org/10.1103/PhysRevB.87.045307, http://link.aps.org/doi/10.1103/PhysRevB.87.045307.
[29] S. Kéna-Cohen, S.A. Maier, D.D.C. Bradley, Ultrastrongly coupled exciton–polaritons in metal-clad organic semiconductor microcavities, Adv. Opt. Mater. 1 (2013) 827, http://dx.doi.org/10.1002/adom.201300256.
[30] S. Gambino, M. Mazzeo, A. Genco, O.D. Stefano, S. Savasta, S. Patane, D. Ballarini, F. Mangione, G. Lerario, D. Sanvitto, G. Gigli, Exploring light–matter interaction phenomena under ultrastrong coupling regime, ACS Photonics 1 (2014) 1042, http://dx.doi.org/10.1021/ph500266d.
[31] T. Schwartz, J.A. Hutchison, C. Genet, T.W. Ebbesen, Reversible switching of ultrastrong light-molecule coupling, Phys. Rev. Lett. 106 (2011) 196405, http://dx.doi.org/10.1103/PhysRevLett.106.196405, http://link.aps.org/doi/10.1103/PhysRevLett.106.196405.
[32] J. Bellessa, C. Symonds, K. Vynck, A. Lemaître, A. Brioude, L. Beaur, J.-C. Plenet, P. Viste, D. Felbacq, E. Cambril, P. Valvin, Giant Rabi splitting between localized mixed plasmon-exciton states in a two-dimensional array of nanosize metallic disks in an organic semiconductor, Phys. Rev. B 80 (2009) 033303, http://dx.doi.org/10.1103/PhysRevB.80.033303, http://link.aps.org/doi/10.1103/PhysRevB.80.033303.
[33] E. Dupont, H.C. Liu, A.J. SpringThorpe, W. Lai, M. Extavour, Vacuum-field Rabi splitting in quantum-well infrared photodetectors, Phys. Rev. B 68 (2003) 245320, http://dx.doi.org/10.1103/PhysRevB.68.245320, http://link.aps.org/doi/10.1103/PhysRevB.68.245320.
[34] L. Sapienza, A. Vasanelli, C. Ciuti, C. Manquest, C. Sirtori, R. Colombelli, U. Gennser, Photovoltaic probe of cavity polaritons in a quantum cascade structure, Appl. Phys. Lett. 90 (2007) 201101.
[35] L. Sapienza, A. Vasanelli, R. Colombelli, C. Ciuti, Y. Chassagneux, C. Manquest, U. Gennser, C. Sirtori, Electrically injected cavity polaritons, Phys. Rev. Lett. 100 (2008) 136806.
[36] Y. Todorov, P. Jouy, A. Vasanelli, L. Sapienza, R. Colombelli, U. Gennser, C. Sirtori, Stark tunable electroluminescence from cavity polariton states, Appl. Phys. Lett. 93 (2008) 171105.
[37] P. Jouy, A. Vasanelli, Y. Todorov, L. Sapienza, R. Colombelli, U. Gennser, C. Sirtori, Intersubband electroluminescent devices operating in the strong coupling regime, Phys. Rev. B 82 (2010) 045322.
[38] A. Delteil, A. Vasanelli, P. Jouy, D. Barate, J. Moreno, R. Teissier, A. Baranov, C. Sirtori, Optical phonon scattering of cavity polaritons in an electroluminescent device, Phys. Rev. B 83 (2011), 081404(R).
[39] M. Geiser, G. Scalari, F. Castellano, M. Beck, J. Faist, Room temperature terahertz polariton emitter, Appl. Phys. Lett. 101 (2012) 141118, http://dx.doi.org/10.1063/1.4757611.
[40] S.D. Liberato, C. Ciuti, Stimulated scattering and lasing of intersubband cavity polaritons, Phys. Rev. Lett. 102 (2009) 136403.
[41] R. Colombelli, J.-M. Manceau, Perspectives for intersubband polariton lasers, Phys. Rev. X 5 (2015) 011031, http://dx.doi.org/10.1103/PhysRevX.5.011031, http://link.aps.org/doi/10.1103/PhysRevX.5.011031.
[42] A. Imamoglu, R.J. Ram, S. Pau, Y. Yamamoto, Nonequilibrium condensates and lasers without inversion: exciton–polariton lasers, Phys. Rev. A 53 (1996) 4250–4253, http://dx.doi.org/10.1103/PhysRevA.53.4250, http://link.aps.org/doi/10.1103/PhysRevA.53.4250.
[43] D. Bajoni, P. Senellart, E. Wertz, I. Sagnes, A. Miard, A. Lemaître, J. Bloch, Polariton laser using single micropillar GaAs-GaAlAs semiconductor cavities, Phys. Rev. Lett. 100 (2008) 047401.
[44] A. Benz, S. Campione, S. Liu, I. Montano, J. Klem, A. Allerman, J. Wendt, M. Sinclair, F. Capolino, I. Brener, Strong coupling in the sub-wavelength limit using metamaterial nanocavities, Nat. Commun. 4 (2013) 2882, http://dx.doi.org/10.1038/ncomms3882.
[45] S. Campione, A. Benz, J.F. Klem, M.B. Sinclair, I. Brener, F. Capolino, Electrodynamic modeling of strong coupling between a metasurface and intersubband transitions in quantum wells, Phys. Rev. B 89 (2014) 165133, http://dx.doi.org/10.1103/PhysRevB.89.165133, http://link.aps.org/doi/10.1103/PhysRevB.89.165133.
[46] D. Dietze, A. Benz, G. Strasser, K. Unterrainer, J. Darmo, Terahertz meta-atoms coupled to a quantum well intersubband transition, Opt. Express 19 (2011) 13700.
[47] J. Lee, M. Tymchenko, C. Argyropoulos, P.-Y. Chen, F. Lu, F. Demmerle, G. Boehm, M.-C. Amann, A. Alù, M.A. Belkin, Giant nonlinear response from plasmonic metasurfaces coupled to intersubband transitions, Nature 511 (2014) 65, http://dx.doi.org/10.1038/nature13455.
[48] S. Campione, A. Benz, M.B. Sinclair, F. Capolino, I. Brener, Second harmonic generation from metamaterials strongly coupled to intersubband transitions in quantum wells, Appl. Phys. Lett. 104 (2014) 131104, http://dx.doi.org/10.1063/1.4870072.
[49] S. Zanotto, F.P. Mezzapesa, F. Bianco, G. Biasiol, L. Baldacci, M.S. Vitiello, L. Sorba, R. Colombelli, A. Tredicucci, Perfect energy-feeding into strongly coupled systems and interferometric control of polariton absorption, Nat. Phys. 10 (2014) 830–834, http://dx.doi.org/10.1038/nphys3106.
[50] T. Laurent, Y. Todorov, A. Vasanelli, A. Delteil, C. Sirtori, G. Beaudoin, I. Sagnes, Superradiant emission from a collective excitation in a semiconductor, Phys. Rev. Lett. 115 (2015) 187402.
[51] M. Helm, Intersubband Transitions in Quantum Wells. Physics and Device Applications I, Semiconductor and Semimetals, vol. 66, Academic Press, 2000.
[52] C. Sirtori, F. Capasso, J. Faist, S. Scandolo, Nonparabolicity and a sum rule associated with bound-to-bound and bound-to-continuum intersubband transitions in quantum wells, Phys. Rev. B 50 (12) (1994) 8663.
[53] T. Ando, A.B. Fowler, F. Stern, Electronic properties of two-dimensional systems, Rev. Mod. Phys. 54 (1982) 437.
[54] L. Wendler, E. Kändler, Intra- and intersubband plasmon–polaritons in semiconductor quantum wells, Phys. Status Solidi B 177 (1993) 9.
[55] G. Pegolotti, A. Vasanelli, Y. Todorov, C. Sirtori, Quantum model of coupled intersubband plasmons, Phys. Rev. B 90 (2014) 035305.
[56] B. Harbecke, B. Heinz, P. Grosse, Optical properties of thin films and the Berreman effect, Appl. Phys. 38 (1985) 263.
[57] A.J. McAlister, E.A. Stern, Plasma resonance absorption in thin metal films, Phys. Rev. 132 (1963) 1599.
[58] Y. Todorov, C. Sirtori, Intersubband polaritons in the electrical dipole gauge, Phys. Rev. B 85 (2012) 045304.
[59] J. Nelayah, M. Kociak, O. Stéphan, F.J.G. de Abajo, M. Tencé, L. Henrard, D. Taverna, I. Pastoriza-Santos, L.M. Liz-Marzán, C. Colliex, Mapping surface plasmons on a single metallic nanoparticle, Nat. Phys. 3 (2007) 348–353, http://dx.doi.org/10.1038/nphys575.
[60] C. Kittel, Quantum Theory of Solids, John Wiley & Sons, New York, 1963.
[61] A.A. Anappara, A. Tredicucci, G. Biasiol, L. Sorba, Electrical control of polariton coupling in intersubband microcavities, Appl. Phys. Lett. 87 (2005) 051105.
[62] Y. Todorov, A.M. Andrews, I. Sagnes, R. Colombelli, P. Klang, G. Strasser, C. Sirtori, Strong light–matter coupling in subwavelength metal–dielectric microcavities at terahertz frequencies, Phys. Rev. Lett. 102 (2009) 186402.
[63] C. Balanis, Antenna Theory Analysis and Design, John Wiley & Sons, Hoboken, New Jersey, 2005.
[64] B.S. Williams, S. Kumar, H. Callebaut, Q. Hu, J.L. Reno, Terahertz quantum-cascade laser at $\lambda = 100$ μm using metal waveguide for mode confinement, Appl. Phys. Lett. 83 (11) (2003) 2124–2126, http://dx.doi.org/10.1063/1.1611642, http://scitation.aip.org/content/aip/journal/apl/83/11/10.1063/1.1611642.
[65] M.J. Adams, An Introduction to Optical Waveguides, John Wiley & Sons, Chichester, 1981.
[66] Y. Todorov, L. Tosetto, J. Teissier, A.M. Andrews, P. Klang, R. Colombelli, I. Sagnes, G. Strasser, C. Sirtori, Optical properties of metal–dielectric–metal microcavities in the frequency range, Opt. Express 18 (13) (2010) 13886–13907, http://dx.doi.org/10.1364/OE.18.013886, http://www.opticsexpress.org/abstract.cfm?URI=oe-18-13-13886.
[67] C. Tsau, S. Spearing, M. Schmidt, Characterization of wafer-level thermocompression bonds, J. Microelectromech. Syst. 13 (6) (2004) 963–971, http://dx.doi.org/10.1109/JMEMS.2004.838393.

[68] P. Jouy, Y. Todorov, A. Vasanelli, R. Colombelli, I. Sagnes, C. Sirtori, Coupling of a surface plasmon with localized subwavelength microcavity modes, Appl. Phys. Lett. 98 (2) (2011) 021105, http://scitation.aip.org/content/aip/journal/apl/98/2/10.1063/1.3536504.
[69] P. Bouchon, C. Koechlin, F. Pardo, R. Haïdar, J.-L. Pelouard, Wideband omnidirectional infrared absorber with a patchwork of plasmonic nanoantennas, Opt. Lett. 37 (6) (2012) 1038–1040, http://dx.doi.org/10.1364/OL.37.001038, http://ol.osa.org/abstract.cfm?URI=ol-37-6-1038.
[70] H.C. Liu, C.Y. Song, Z.R. Wasilewski, A.J. SpringThorpe, J.C. Cao, C. Dharma-wardana, G.C. Aers, D.J. Lockwood, J.A. Gupta, Coupled electron–phonon modes in optically pumped resonant intersubband lasers, Phys. Rev. Lett. 90 (2003) 077402, http://dx.doi.org/10.1103/PhysRevLett.90.077402, http://link.aps.org/doi/10.1103/PhysRevLett.90.077402.
[71] B. Askenazi, et al., in preparation.
[72] F. Alpeggiani, L.C. Andreani, Semiclassical theory of multisubband plasmons: nonlocal electrodynamics and radiative effects, Phys. Rev. B 90 (2014) 115311, http://dx.doi.org/10.1103/PhysRevB.90.115311, http://link.aps.org/doi/10.1103/PhysRevB.90.115311.
[73] R.H. Dicke, Coherence in spontaneous radiation process, Phys. Rev. 93 (1954) 99.
[74] N. Skribanowitz, I.P. Herman, J.C. MacGillivray, M.S. Feld, Observation of Dicke superradiance in optically pumped HF gas, Phys. Rev. Lett. 30 (1973) 309–312, http://dx.doi.org/10.1103/PhysRevLett.30.309, http://link.aps.org/doi/10.1103/PhysRevLett.30.309.
[75] A. Goban, C.-L. Hung, J.D. Hood, S.-P. Yu, J.A. Muniz, O. Painter, H.J. Kimble, Superradiance for atoms trapped along a photonic crystal waveguide, Phys. Rev. Lett. 115 (2015) 063601, http://dx.doi.org/10.1103/PhysRevLett.115.063601, http://link.aps.org/doi/10.1103/PhysRevLett.115.063601.
[76] M. Scheibner, T. Schmidt, L. Worschech, A. Forchel, G. Bacher, T. Passow, D. Hommel, Superradiance of quantum dots, Nat. Phys. 3 (2007) 106, http://dx.doi.org/10.1038/nphys494.
[77] H. Fidder, J. Knoester, D.A. Wiersma, Superradiant emission and optical dephasing in j-aggregates, Chem. Phys. Lett. 171 (5–6) (1990) 529–536, http://dx.doi.org/10.1016/0009-2614(90)85258-E, http://www.sciencedirect.com/science/article/pii/000926149085258E.
[78] A.F. van Loo, A. Fedorov, K. Lalumière, B.C. Sanders, A. Blais, A. Wallraff, Photon-mediated interactions between distant artificial atoms, Science 342 (6165) (2013) 1494–1496, http://dx.doi.org/10.1126/science.1244324, arXiv: http://science.sciencemag.org/content/342/6165/1494.full.pdf, http://science.sciencemag.org/content/342/6165/1494.
[79] Q. Zhang, T. Arikawa, E. Kato, J.L. Reno, W. Pan, J.D. Watson, M.J. Manfra, M.A. Zudov, M. Tokman, M. Erukhimova, A. Belyanin, J. Kono, Superradiant decay of cyclotron resonance of two-dimensional electron gases, Phys. Rev. Lett. 113 (2014) 047601, http://dx.doi.org/10.1103/PhysRevLett.113.047601, http://link.aps.org/doi/10.1103/PhysRevLett.113.047601.
[80] S. Huppert, A. Vasanelli, T. Laurent, Y. Todorov, G. Pegolotti, G. Beaudoin, I. Sagnes, C. Sirtori, Radiatively broadened incandescent sources, ACS Photonics 2 (12) (2015) 1663–1668, http://dx.doi.org/10.1021/acsphotonics.5b00415.
[81] S. Morina, O.V. Kibis, A.A. Pervishko, I.A. Shelykh, Transport properties of a two-dimensional electron gas dressed by light, Phys. Rev. B 91 (2015) 155312, http://dx.doi.org/10.1103/PhysRevB.91.155312, http://link.aps.org/doi/10.1103/PhysRevB.91.155312.
[82] C.S. Colley, J.C. Hebden, D.T. Delpy, A.D. Cambrey, R.A. Brown, E.A. Zibik, W.H. Ng, L.R. Wilson, J.W. Cockburn, Mid-infrared optical coherence tomography, Rev. Sci. Instrum. 78 (2007) 123108, http://dx.doi.org/10.1063/1.2821609.
[83] R. Colombelli, C. Ciuti, Y. Chassagneux, C. Sirtori, Quantum cascade intersubband polariton light emitters, Semicond. Sci. Technol. 20 (2005) 985.
[84] J. Faist, F. Capasso, D.L. Sivco, C. Sirtori, A.L. Hutchinson, A.Y. Cho, Quantum cascade laser, Science 264 (1994) 553, http://dx.doi.org/10.1126/science.264.5158.553.
[85] S. Fathololoumi, E. Dupont, C. Chan, Z. Wasilewski, S. Laframboise, D. Ban, A. Mátyás, C. Jirauschek, Q. Hu, H.C. Liu, Terahertz quantum cascade lasers operating up to ≈ 200 K with optimized oscillator strength and improved injection tunneling, Opt. Express 20 (2012) 3866.